Arabian Journal of Chemistry (2022) **15**, 103970

King Saud University

**Arabian Journal of Chemistry**

www.ksu.edu.sa
www.sciencedirect.com

ORIGINAL ARTICLE

# *Astragalus membranaceus* ultrafine powder alleviates hyperuricemia by regulating the gut microbiome and reversing bile acid and adrenal hormone biosynthesis dysregulation

**Wenwen Zhang [a], Yifang Cui [b], Zihan Liu [c], Shaoping Wang [a], Ailin Yang [a], Xiulian Li [a], Jiayu Zhang [a,*]**

[a] *The Faculty of Pharmacy, Binzhou Medical University, China*
[b] *The Faculty of Pharmacy, Shandong University of Traditional Chinese Medicine, China*
[c] *The Faculty of Pharmacy, Beijing University of Traditional Chinese Medicine, China*

Received 6 January 2022; accepted 16 May 2022
Available online 25 May 2022

**KEYWORDS**

Hyperuricemia;
*Astragalus membranaceus* ultrafine powder;
Drug metabolism;
Gut microbiome;
Feces metabolomic

**Abstract** *Ethnopharmacological relevance:* Metabolic syndrome is closely related to the intestinal microbiota and disturbances in the host metabolome. Hyperuricemia (HUA), a manifestation of metabolic syndrome, can induce various cardiovascular diseases and gout, seriously affecting a patient's quality of life. *Astragalus membranaceus* has a long history as a commonly used traditional Chinese medicine to treat kidney disease in China and East Asia.

*Materials and methods:* We compared the therapeutic effect of benzbromarone and two different doses *Astragalus membranaceus* ultrafine powder (AMUP) in rats with HUA. Ultra-performance liquid chromatography-mass spectrometer was used to analyze the AMUP metabolism in the plasma, urine, and feces. Further, 16S ribosome RNA sequencing and feces metabolomic were performed to capture the variation of the gut microbiota and metabolites changes before and after drug administration.

*Results:* AMUP had a notable impact on reducing blood uric acid levels while protecting the liver and kidney. Drug metabolism analysis demonstrated that effective constituent flavonoids are distributed in the blood, whereas saponins remain in the intestine. Gut microbiota analysis showed that low-dose AMUP ameliorated HUA-induced gut dysbiosis by reducing the abundance

* Corresponding author at: The Faculty of Pharmacy, Binzhou Medical University, Guan Hai Road, YanTai, Shandong 264003, China.
E-mail address: zhangjiayu0615@163.com (J. Zhang).

Peer review under responsibility of King Saud University.

Production and hosting by Elsevier

https://doi.org/10.1016/j.arabjc.2022.103970

of harmful bacteria and increasing that of some beneficial bacteria with anti-inflammatory properties, such as Clostridia, Lachnospiraceae, and Muribaculaceae. In addition, HUA-induced changes in metabolite contents in bile acid and adrenal hormone biosynthesis pathways were restored after treatment with AMUP.

*Conclusion:* Low-dose AMUP exerts remarkable therapeutic effects on HUA by regulating the gut microbiome and mediating gut metabolism pathways associated with uric acid excretion.



## 1. Introduction

Hyperuricemia (HUA) is a metabolic disease caused by the continuous purge associated with purine metabolism disorders and a decrease in uric acid excretion (Murea 2012). HUA is an important risk factor for chronic kidney disease, cardiovascular disease (Li et al. 2019), and gouty arthritis (Li et al. 2015). However, the role of urate-lowering therapies in HUA complicated by renal damage remains controversial (Hu and Wu 2019). Recent mounting evidence suggests a causal relationship between the gut microbiota and development of HUA.(Ussar et al. 2015, Wang and Zhao 2018, Liu et al. 2020). These effects may be mediated in part by the gut metabolome because many bacterial species regulate the biosynthesis, biolysis, and transport of metabolites (Pedersen et al. 2016). However, little research has focused on whether "drugging the microbiome" is adequate for HUA treatment.

*Astragalus membranaceus* (Fisch.) Bunge (Huangqi, AM) is one of the most critical Qi-tonifying adaptogenic herbs in traditional Chinese medicine (TCM) and has a long history of medicinal use (Sinclair 1998, Xu et al. 2008, Fu et al. 2014, Liu et al. 2017). Pharmacological studies continue to substantiate claims that AM has the effect of reducing serum creatinine, albuminuria excretion, glomerular filtration and mesangial thickness in diabetic nephropathy(Li et al. 2011) and suppresses the apoptosis of glomerular podocytes (Yang et al. 2020). In addition, the major effective constituents of AM are polysaccharides, flavonoids, and saponins, many of which are potential substrates for the gut microbiota (Lyu et al. 2017). However, the critical mechanism underlying the metabolic protective impact of these components remains unclear.

In this study, we discovered that low and high doses of AMUP reduced serum uric acid levels and protected liver and kidney tissues. In addition, we identified the possible AM components that played pharmacodynamic roles in the blood and intestine by analyzing drug metabolites. Else, using 16S ribosomal RNA (rRNA)–based microbiota analysis and feces metabolomics profiling, we demonstrate that low-dose AMUP treatment alleviates HUA-induced gut dysbiosis and reverses the dysregulation of metabolic pathways in rats with HUA.

## 2. Materials and methods

### 2.1. AMUP

Wild dried root of *Astragalus membranaceus* (Fisch.) Bunge was obtained from Shanxi Hunyuan, Wansheng Astragalus Development Co., Ltd. The AM roots were cut into segments ~2–3 cm long and baked in an oven at 60 °C for 4 h. After drying, the segments were crushed using an ultrafine grinder and then screened through a 400-mesh sieve to obtain AMUP.

### 2.2. Animals, drug administration, and biological sample collection and preparation

Pathogen-free male Sprague–Dawley rats (weight 180–220 g) were obtained from Jinan Pengyue Experimental Animal Breeding Company (license number: SCXK [LU] 20190003). Animal experiments were conducted in accordance with the internationally accepted principles for laboratory animal use and care as found in for example the European Community guidelines (EEC Directive of 1986; 86/609/EEC). The rats were raised in an animal quarter at a temperature of 22 ± 2 °C with 12-h light/12-h dark cycle and 50 ± 10% humidity.

The rats were randomly divided into a blank control group (BC group), HUA model group (Model group), positive drug (benzbromarone) group (Ben group), low-dose AMUP group (LA group), and high-dose AMUP group (HA group). The rats were then labeled and weighed. Before the day of administration, the rats were fasted for 12 h but allowed access to water. The rats in the five groups were given the following intervention measures: the BC group was not given any intervention; the other four groups received intragastric administration of 300 $mg{\cdot}kg^{-1}$ potassium oxonate at 8:00 every morning and fed 10% fructose water. After that, Ben group, LA group and HA group received intragastric administration twice daily (9 AM and 4:00 PM) every day for 24 days of 20 $mg{\cdot}kg^{-1}$ benzbromarone solution, 1.5 $g{\cdot}kg^{-1}$ AMUP, or 3 $g{\cdot}kg^{-1}$ AMUP, respectively. All drugs were dispersed in 10 mL of distilled water. The BC group was gavaged with the same volume of water. All the animals in the five groups had normal forage.

All rats were weighed every 12 days. Fresh feces were obtained by stimulating the anus. Blood samples were collected by *retro*-orbital bleed into heparinized tubes at different time points according to experiment needs and then immediately centrifuged at 13,00*g* for 10 min to obtain plasma. All rats were put into metabolic cages for urine and feces sample collection. All samples were stored at −80 °C for later analysis.

The rats were fasted on the 24th day after administration and anesthetized by intraperitoneal injection of 10% chloral hydrate 3 h after the last administration. Surgical scissors and forceps were used to remove the liver and kidney tissues. Blood was removed by washing with normal saline, and then the water on the surface of the tissue was removed using absorbent paper, and the tissue was then soaked in 4% paraformaldehyde, and hematoxylin-eosin (HE) staining was conducted for pathological analysis according to a previous report (Fischer et al. 2008).

Some blood samples were used for uric acid (UA), glucose (Glu), triglyceride (TGs), alanine aminotransferase (ALT), aspartate aminotransferase (AST), indirect bilirubin (IBIL) measurements using a UA assay kit (Abcam, ab65344), Glu assay kit (Abcam, ab65333), triglyceride assay kit (Abcam, ab65336), Alanine Transaminase Activity assay kit (Abcam, ab105134), Aspartate Aminotransferase Activity assay kit (Abcam, ab105135), and Bilirubin assay kit (Abcam, ab235627), respectively. Plasma samples for Ultra performance liquid chromatography-mass spectrometer (UPLC–MS) analysis were prepared according to a previous report, with minor modifications (Liu et al. 2017). Each plasma sample (1 mL) was precipitated with 3 mL of methanol. After vortexing for 1 min, the sample was centrifuged at 3000 rpm for 10 min. The organic layer was then transferred to a fresh tube and evaporated to dryness. The residue was reconstituted in 1 mL of methanol and centrifuged at 13,000 rpm for 10 min.

Frozen urine and stool samples were thawed at room temperature. Treatment of urine and feces was carried out according to a previous report (Wikoff et al. 2009). One volume of each urine sample was added to 3 volumes of methanol, and stool samples were extracted twice with 6 times the amount of methanol. Samples were centrifuged at 13,000 g for 10 min and filtered through a 0.22-μm membrane filter in preparation for liquid chromatography-mass spectrometry (LC–MS) analysis. Finally, 2 μL of the supernatant was injected into the UPLC–MS system for analysis.

Some feces samples were stored at −80 °C and used for analysis of the gut bacterial community and fecal metabolomics.

### 2.3. Instrumentation and UPLC–MS conditions

Chromatographic experiments were performed on a Waters ACQUITY UPLC system (Waters Corp., Milford, MA, USA) according to a previous report, with minor modifications (Zhao et al. 2017). UPLC separation was achieved on a Syncronis C18 column (100 mm × 2.1 mm i.d., 1.7 μm; Thermo, US), with the column temperature set at 35 °C. The gradient condition of the mobile phase was as follows: B increased from 3% to 97% over 9 min. The flow rate was 0.4 mL/min, and the injection volume was 2 μL. The MS instrument consisted of a Waters ACQUITY Synapt QTOF/MS (Waters Corp.). Ionization was performed in the negative electrospray (ESI) mode. The temperature of the ion source was maintained at 120 °C, and the desolvation temperature was 320 °C. The flow rates of cone and desolvation gas ($N_2$) were 50 and 600 L/h, respectively. The capillary voltage used for the analysis of catalpol and its metabolites was 3.2 kV. All data collected in centroid mode were acquired using MasslynxNT 4.1 software (Waters Corp.).

### 2.4. 16S rRNA gene sequence analysis

Microbial genomic DNA was extracted from fecal pellets using a PowerSoil DNA Isolation kit (MOBIO Laboratories) according to the manufacturer's protocols, and samples were stored at −80 °C until further testing. DNA quality and quantity were assessed by determining the absorbance ratios at 260 nm/280 nm and 260 nm/230 nm, respectively. The V3 + V4 sequenced regions of the 16S rRNA gene were amplified by PCR using universal primers. DNA libraries for Illumina sequencing were constructed using a NEBNext Ultra Directional RNA Library Prep kit for Illumina (E7420) following the manufacturer's instructions. DNA library quality was assessed using an Agilent High-Sensitivity DNA Chip.

### 2.5. Read mapping and data analysis

Raw data were processed according to previous reports, with minor modifications (Chen et al. 2019, Johnson et al. 2019). The raw data files were converted into FASTQ file format by Base Calling Analysis. Paired-end sequence data were merged into one sequence of Tags. FLASH v1.2.7 software was used to splice the reads of each sample via overlap. Trimmomatic v0.33 software was used to filter the raw tags to obtain high-quality tag data. Chimeric sequences were identified and removed using UCHIME v4.2 software to obtain the effective tags. Clustering of tags at the 97% sequence similarity level using UCLUST in QIIME (version 1.8.0) software was carried out to obtain operational taxonomic units (OTUs), and the OTUs were taxonomically annotated based on the Silva (bacteria, https://www.arbsilva.de) and UNITE (fungi, https://unite.ut.ee/index.php) taxonomic databases. OTUs were filtered using 0.005% of all sequence numbers as a threshold. The OTU representative sequences were compared with the microbial reference database to obtain the species classification information corresponding to each OTU, and then the composition of each sample was determined at each level (i.e., phylum, class, order, family, genus, species). On this basis, QIIME software was used to generate a species abundance table at different classification levels, and R package was used to map the community structure plot under the taxonomic level of the sample. Species annotation was performed using the RDP Classifier (version 2.2, https://sourceforge.net/projects/rdpclassifier/) with a confidence threshold of 0.8. Alpha diversity of samples (Rarefaction curve, Shannon index, Rank abundance curve, Chao1 richness estimator, Ace richness estimator, Simpson diversity index, etc.) was determined using Mothur software (version v.1.30). Beta diversity analysis was performed using the Bray-Curtis algorithm of QIIME and R software to compare the similarity of species diversity in different samples. Finally, analysis of variance was performed to screen species with significant differences at the genus level ($P < 0.05$).

### 2.6. Fecal metabolomic and data analyses

Fecal metabolomic samples were treated according to a previous report, with some modifications (Le Gall et al. 2011). First, 250 mg of each stool sample was thawed at room temperature, after which 1 mL of phosphate-buffered saline (0.2 mol/L $Na_2HPO_4$/ $NaH_2PO_4$ [pH 7.4]) was added to the sample and centrifuged at 14,000 rpm and 4 °C for 10 min. Thereafter, 400 μL of the supernatant and 100 μL of $D_2O$ (containing 0.05% sodium salt tri-methysilypropionic acid) were mixed together and transferred into a 5-mm nuclear magnetic tube and stored in a refrigerator at 4 °C for 5 h. All fecal sample spectra were processed at 298 K using a Bruker spectrometer (Avance III 500 MHz) with a one-dimensional water presaturated standard NOESYPR1D pulse sequence (recycle delay-90-t1-90-tm-90-acquisition). The pretreated data were uploaded into

SIMCA-P (version 14.1, Umetrics, Umea, Sweden) for multivariate data analysis. Intensity values with an invalid result (NA) were replaced by zero. Peak intensity was calibrated by total intensity. Variates with a relative standard deviation ≥40% in quality controls were excluded. The final matrix was exported to an EXCEL file for further processing.

Orthogonal partial least-squares discriminant analysis (OPLS-DA) is a statistical method of supervised discriminant analysis. The grouping variables are included in the modeling for pair-wise analysis to make group differences and differences between two metabolic profiles clearer, thus enabling the screening of different metabolites. Twenty recalculated permutations were used to evaluate the validity of the model. The variable importance in the projection (VIP) value of each variable in the OPLS-DA model was calculated to indicate its contribution to the classification. Metabolites with a VIP value $>1$ as well as $|p(corr)| > 0.3$ were further evaluated using the Mann–Whitney $U$ test to determine the significance of each metabolite, with $P < 0.05$ considered statistically significant. A heatmap plot and bar plot were constructed using the R package program. Metabo Analyst 5.0 database (https://www.MetaboAnalyst.ca/) was used for the pathway analysis.

## 3. Results and discussion

### 3.1. AMUP exhibits potential protective effects on the kidney and liver

To evaluate the UA–reducing pharmacodynamic activity and protective effect of AMUP on liver and kidney tissue, we measured the UA concentration in the serum of rats at 12 days and 24 days after gavage. The results suggested that the serum UA level of rats in the HUA model group was significantly higher than that in the BC group (Fig. 1A), confirming that HUA model construction was successful. This increase was reversed in the Ben group and the AMUP groups. Interestingly, the treatment effect of AMUP was better than that of the positive control drug (Fig. 1A).

High UA levels cause renal injury and can even lead to acute and chronic kidney disease (Cote et al. 2020, Liu et al. 2021). Analysis of HE staining of kidney tissues of the rats in the control blank groups under 100 × light microscopy revealed that the renal tubules were normal in shape, complete in structure, and orderly arranged, and there was no inflammatory cell infiltration in the tubulointerstitium (Fig. A.1). In contrast, images of the model group showed that the renal tubules were damaged and exhibited tubulodilatation and inflammatory cell infiltration in the tubulointerstitium. However, pathological changes were also found in kidney tissues after treatment with benzbromarone, indicating that this drug may only reduce the UA level to some extent but not reverse organ damage caused by HUA or benzbromarone itself, as this drug does exhibit kidney toxicity (Fig. A.1). Two clinical cases also showed that benzbromarone can cause acute kidney injury following self-medication for HUA (Ye et al. 2019). AMUP at both low and high doses can alleviate such physiological changes in organs, suggesting that AMUP has a significant effect on reducing UA levels and reversing the kidney damage caused by HUA.

ALT, AST, and IBIL are important indicators of liver health (Kwo et al. 2017). As shown in Fig. 2A–C, the levels of ALT and AST, as well as IBIL, were higher in the model group than the BC group, suggested that HUA can cause liver damage. In contrast, the serum levels of ALT, AST, and IBIL decreased after treatment with AUMP or benzbromarone. Consistently, no inflammatory cell infiltration, degeneration, fibrosis, necrosis, or other pathological changes were observed in blank controls (Fig. A.2). However, in the model group, the structure of the hepatic lobules and the shape of the vacuoles in the cytoplasm of hepatocytes were altered, and some cells were larger and others exhibited a compressed nucleus. Pathological changes in liver tissue were reversed in the AUMP treatment groups but not in the benzbromarone group, demonstrating that benzbromarone cannot repair organ damage caused by HUA. This observation was consistent with a reported clinical case of an HUA patient treated with benzbromarone who developed severe liver injury after 26 days (Zhang et al. 2019).

Other important pathological indexes, such as TG and Glu levels, have also been evaluated in rats (Alves-Bezerra and Cohen 2017, Qi and Tester 2019). Levels of TGs and Glu were also significantly elevated in the model group (Fig. 1B), suggesting that HUA is also associated with diseases such as diabetes and hyperlipidemia and that AUMP may have potential to relieve the complications of these diseases.

### 3.2. Transformation of AMUP to characteristic metabolites

Metabolism refers to the process by which the chemical structure of a compound changes under the action of a variety of metabolizing enzymes and is a major determinant of the clinical efficacy, clearance, and toxicity of a drug (Lu 2007). After administration, drug metabolism primarily occurs in the intestines mediated by the gut microbiota. In this process, the drug usually undergoes chemical modification, producing metabolites that can have different functional and toxicological properties compared to those of the precursor. Some drug components or metabolites in the gut are absorbed by the intestinal epithelium and enter the blood and travel to organs, where additional metabolic reactions may take place. Unabsorbed components or metabolites are excreted from the body via the urine and feces.

To identify the active component of low-dose AMUP treatment in the metabolic process *in vivo*, we analyzed AMUP metabolites in plasma, feces, and urine by LC–MS. A total of eight chemical components were detected in plasma (Table A1). Among these components, seven prototype constituents, including two calycosin isomers, a daidzein isomer, odoratin-7-*O*-*β*-*D*-glucoside isomer, 5,7,4′-trihydroxy-isoflavo none isomer, formononetin isomer, and 3,9-dimethoxy-10-hy droxypterocarpan isomer were identified. One of the metabolites of AMUP in plasma is the product of isomucronulatol glucuronidation. Isomucronulatol-7-*O*-*β*-*D*-glucoside exhibits anti-osteoarthritic effects (Hong et al. 2018) by reducing the expression of all osteoarthritis-related molecules (Hong et al. 2018), suggesting that the products of isomucronulatol glucuronidation may play a role in the effects of HUA treatment.

We also analyzed the metabolites in feces and urine and identified 31 compounds in supernatant of feces (Table A2), most of which were saponins. These 31 compounds included 15 isomers of prototypical compounds and 16 prototypical transformation components of methylation, carboxylation,

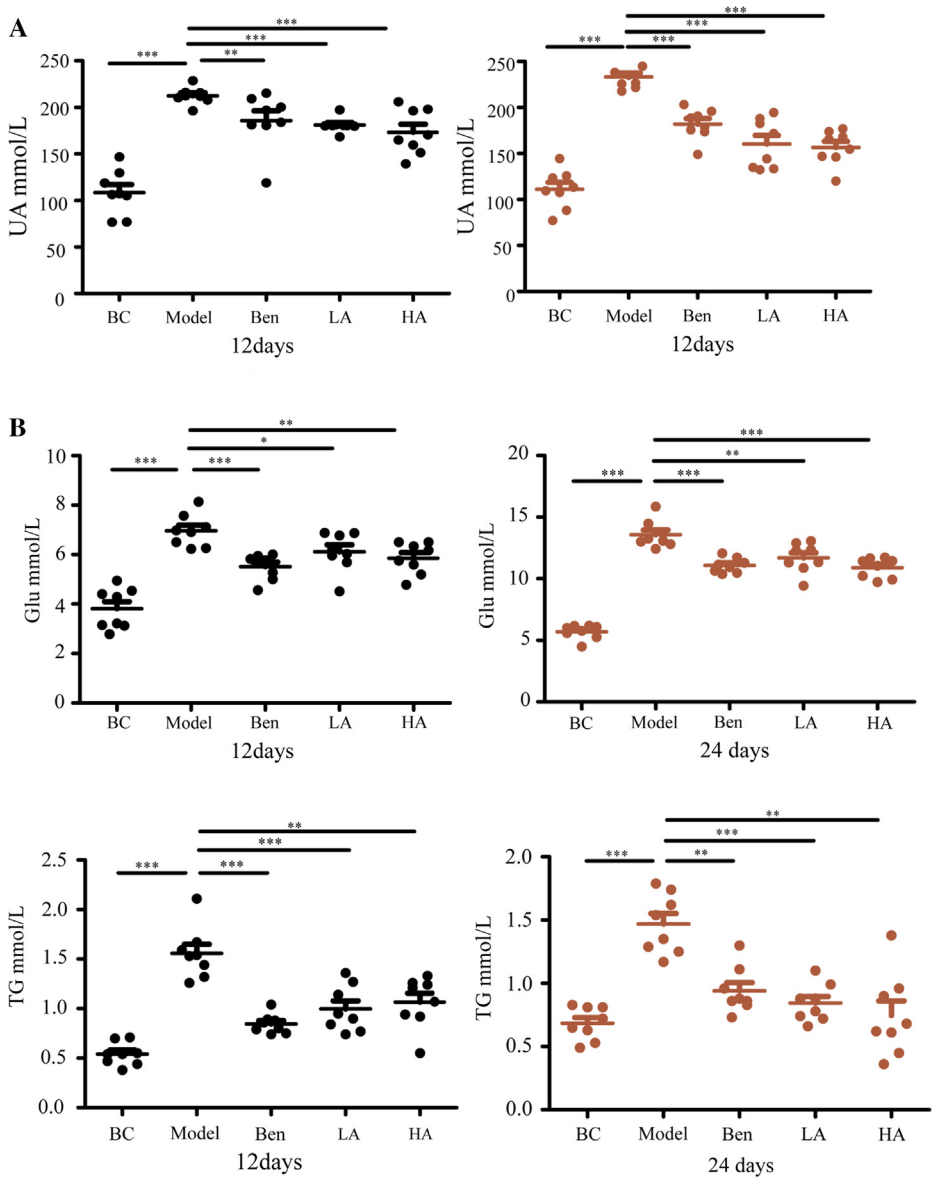


**Fig. 1** AMUP has obvious effect in the treatment of HUA. A, AMUP has the same effect in reducing uric acid levels as benzbromarone in rats with HUA 12 and 24 days after administration. B, AMUP treatment decreased the Glu and TG levels of the rats with HUA on days 12 and 24. *P* values were determined by paired *t*-test (*$P < 0.05$;**$P < 0.01$;***$P < 0.001$).

and hydroxylation. A total of 38 chemical components were identified in urine (Table A3), including 27 prototypical compounds and 11 prototypical transformation components. Unlike the metabolites in feces, most of the components in urine were flavonoids. The prototypical transformation components primarily consisted of glucuronidation, hydroxylation, and methylation products. Taken together, these results suggest that flavonoids exert therapeutic effects in the blood, whereas saponins and their metabolic components are not easily absorbed into the blood to exert therapeutic effects. However, saponins can play a specific role in regulating the community structure of the intestinal flora (Kim 2018, Xu et al. 2020). This result suggested that different components of TCM may exhibit the pharmacodynamic effect at different body parts via different mechanisms.

### *3.3. AMUP ameliorates HUA-induced gut dysbiosis*

Recent explorations of the interplay between phytochemicals and the gut microbiota have revolutionized our understanding of the underlying mechanisms (Sanchez et al. 2017). The gut microbiota plays a pathogenic role in the development of cardiovascular disease (Tang et al. 2017). As modulation of the microbiome is a potential therapeutic approach for HUA treatment, we examined the effects of AMUP on the gut microbiota composition by performing a pyrosequencing-based analysis of bacterial 16S rDNA in feces. A random sampling method was used to construct a rarefaction curve, which indicated that the sequencing data were reasonable for further analysis (Fig. A.3B). The alpha diversity of fecal microbiota for five groups as measured by the Shannon index showed that

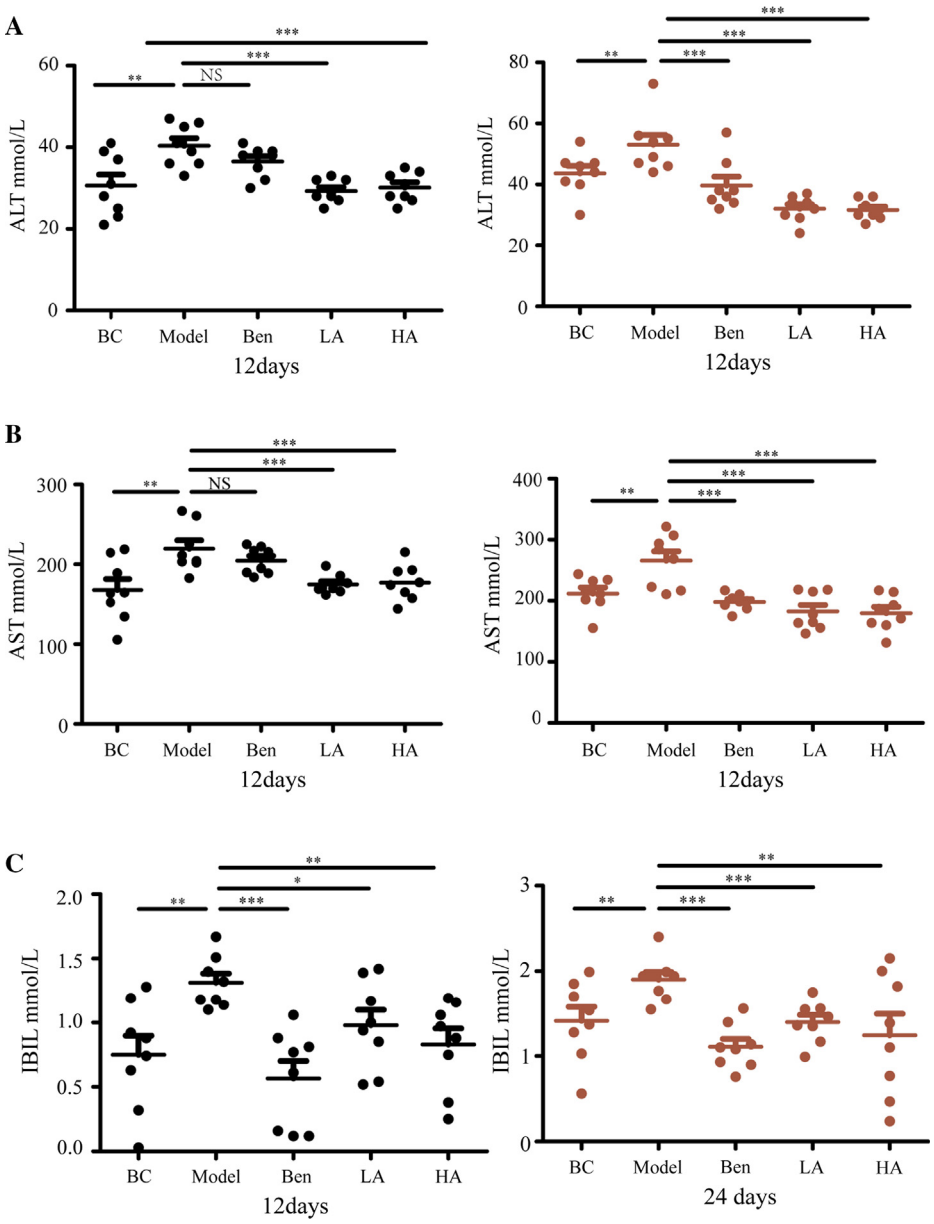


**Fig. 2** AMUP functions in protecting the liver in rats with HUA. A-C AMUP decreased ALT, AST, and IBIL levels in rats with HUA after 12 and 24 days of treatment. *P* values were determined by paired *t*-test (*$P < 0.05$; **$P < 0.01$; ***$P < 0.001$).

there was no significant difference in composition between HUA rats treated with AUMP and the BC group (Fig. 3A). However, significant differences were observed between the model group and BC group as well as the benzbromarone group and BC group. This result indicates that the intestinal microbiota structure of rats with HUA after treatment with AMUP is similar to that of normal rats.

We also observed a distinct clustering of microbiota composition for five groups using binary_jaccard–based principal co-ordinate analysis (PCoA). The PCoA of the BC and model groups revealed the dysbiosis caused by HUA (Fig. 3B), and the microbiome of the positive, low-dose, and high-dose AMUP groups became more similar to that of the blank control group. This result suggests that AMUP treatment can restore the microbiota in HUA rats to a certain extent.

To assess the overall composition of the bacterial community in the different groups, we analyzed the degree of bacterial taxonomic similarity at the phylum level. High concentrations of uric acid in the intestine led to an increase in the ratio of Firmicutes (Yokota et al. 2012) compared with the BC group. In addition, model negative group rats displayed a significant increase in the relative abundance of Firmicutes and a higher Firmicutes-to-Bacteroidetes ratio, whereas the positive group and low-dose and high-dose AMUP groups were protected against this effect to a large extent (Fig. 3D and Fig. A.3C). It has been reported that a higher Firmicutes-to-

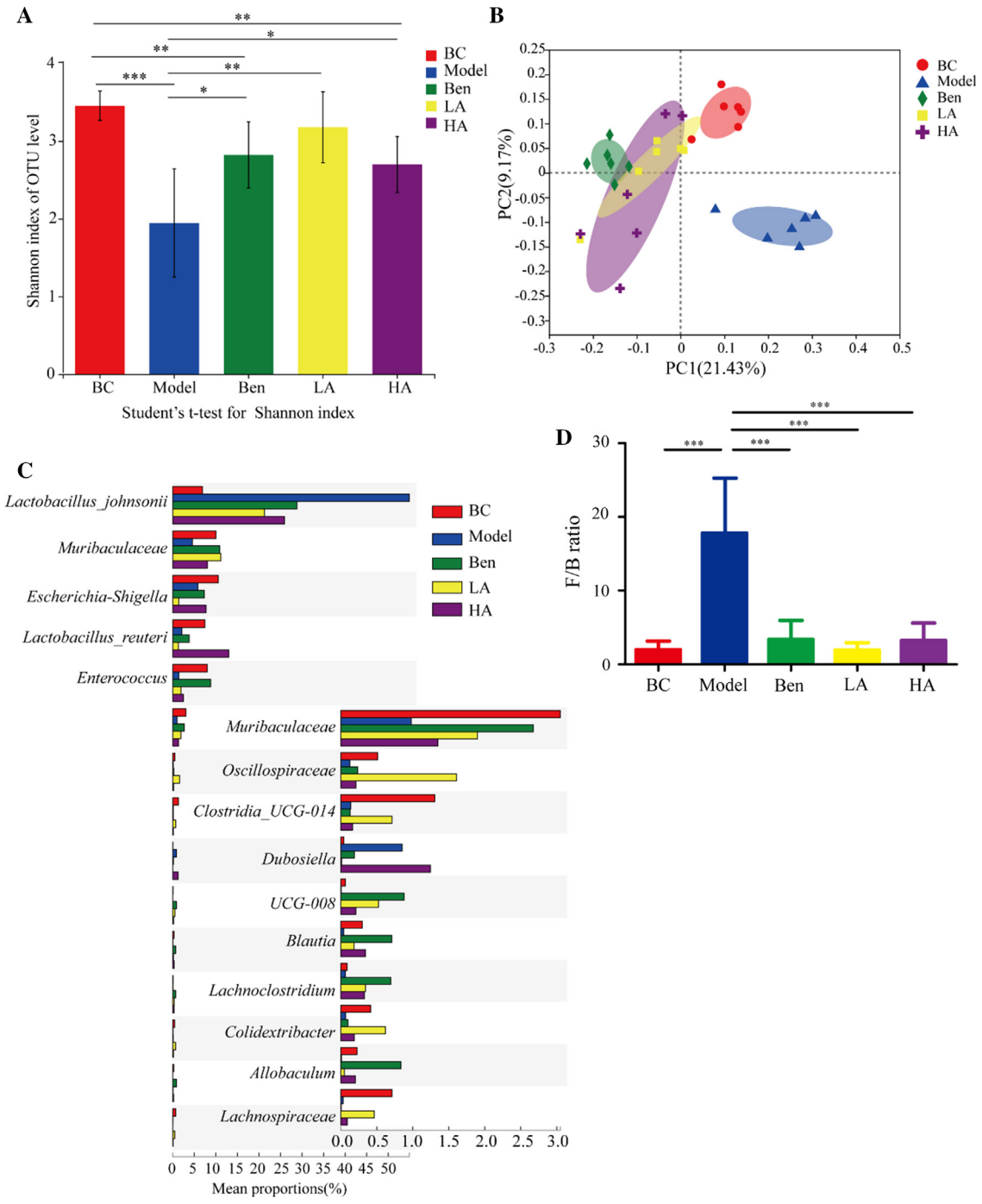


**Fig. 3** AMUP treatment ameliorated HUA-induced gut dysbiosis in rats. A, Alpha-diversity of fecal microbiota for the five groups as measured by the Shannon index. B, Weighted UniFrac PCoA analysis of gut microbiota based on the OTU data for the five groups. C, Top 15 strains that showed significant differences in abundance based on Kruskal–Wallis *H* test. D, Firmicutes-to-Bacteroidetes ratio in the indicated groups. Data are expressed as mean ± SD, and *P* values were determined by paired *t*-test (**P* < 0.05;***P* < 0.01; ****P* < 0.001).

Bacteroidetes ratio in the microbiome is associated with higher body weight, which is also consistent with our observation (Fig. A.3A).

The results of 16S rRNA sequencing analyses confirmed that the microbiome community structure of rats treated with the low dose of AMUP was more similar to that of healthy rat microbiomes than that of the microbiomes of the ben and HA group. This result also suggested that even if benzbromarone is used in HUA treatment, it cannot reverse the structural disorder of the intestinal flora caused by HUA. The microbiome of rats treated with a high-dose of AMUP was significantly different compared with that of healthy rats, which may have been because, like many other medicines, high doses of AMUP can exhibit certain toxic side effects.

To investigate species showing differences in the abundance of microbial community groups, Kruskal–Wallis *H* test–based hypothesis testing was conducted at the species level. We screened the top 15 strains that exhibited significant differences in abundance, but most of these remain unclassified and uncultured. As Fig. 3C shows, *Lactobacillus johnsonii* was present in markedly higher abundance in the model group compared with other fours groups. Although *Lactobacillus johnsonii* is a probiotic species that is beneficial in obese patients, helping to reduce body fat and alleviate diabetes in rats (Teixeira et al. 2018), a too high an abundance of *Lactobacillus johnsonii* may be indicative of an intestinal flora disorder.

The abundance of Muribaculaceae in the gut of the model group decreased significantly compared with the BC group but recovered to the normal abundance after treatment with benzbromarone or AMUP. Muribaculaceae species contribute to the production of propionate (Smith et al. 2019), a short-chain fatty acid that is a major microbial fermentation metabolite in the human gut (Hosseini et al. 2011). Propionate is thought to lower lipogenesis (Nishina and Freedland 1990), serum cholesterol levels (Lin et al. 1995), and inhibit carcinogenesis (Milovic et al. 2000) and extend life span in rats (Sibai et al. 2020). Therefore, a high abundance of Muribaculaceae may have the potential to relieve HUA by increasing the intestinal propionate concentration.

*Shigella* is a bacterial pathogen that causes typical bacillary dysentery (Baker and The 2018, Liu et al. 2019). The abundance of *Shigella* was lower in the low-dose AMUP treatment group than the other three groups, suggesting that a lower abundance of *Shigella* contributed to the observed similarity in the microbial communities of the low-dose AMUP and BC groups. The Clostridia have many roles. *Clostridium butyricum* ameliorates excessive intestinal inflammation by reducing the production of interleukin (IL)-1β and IL-6 (Zhao et al. 2019). Both animal models and clinical trials revealed that members of the Clostridia help prevent or resolve allergic symptoms (Shu et al. 2019). A recent study reported the use of Clostridia stains in cancer therapy (Minton 2003). The results of 16s rRNA sequencing showed that the abundance of Clostridia species in the rat intestine matched that of the BC group only in the low-dose AUMP treatment group, suggesting that low-dose AMUP may support the growth of Clostridia.

A previous analysis of the gut microbiota reported that obese people have fewer *Allobaculum* species in the intestine (Kong et al. 2019). In our study, *Allobaculum* was almost undetectable in the model group, suggesting that model group rats should exhibit increased weight. Indeed, the weight of rats in the model group was generally higher than that of rats in the other groups (Fig. A.3A). Lachnospiraceae, a family of tricillonitaceae, is known to be involved in the development of metabolic disorders (Meehan and Beiko 2014), diabetes (Qin et al. 2012), and restricting intestinal inflammation via the production of butyric acid (Chen et al. 2017, Wallace et al. 2019). A decreased abundance of Lachnospiraceae was found in feces of the model and bromobenzene groups, whereas the Lachnospiraceae abundance in rats of the low-dose AMUP group was similar to that of the BC group, suggesting that the risk of intestinal inflammation and metabolic disorders would be higher in HUA patients and that low-dose AUMP treatment could reduce this risk. The function of members of the genus *Blautia*, which was identified in the human gut, remains unclear. However, we found that the abundance of *Blautia* was significantly deceased in rats with HUA but similar in the other three groups, suggesting that *Blautia* may play a role in HUA treatment.

### 3.4. AMUP intervene metabolomics

The potential utility of metabolomics analysis in the early diagnosis of disease, drug safety evaluations, and personalized toxicology research has been demonstrated in several studies (Ussher et al. 2016, Lains et al. 2019). As the intestinal microbial community in rats with HUA was affected by AUMP, we hypothesized that the metabolome in the feces of rats with HUA would be altered by AUMP treatment. To explore the potential protective mechanism of AUMP on HUA, feces metabolomics analyses were performed using LC–MS. Principal component analysis models containing all quality control, BC, and model samples were first established to observe the clustering of quality controls as well as the distance between the BC and model groups (Fig. A.4A and A.4B). Quality controls clustered closely no matter whether in positive (Fig. A.4A) or negative (Fig. A.4B) mode, which indicated satisfactory reproducibility and stability of the acquisition system. In addition, samples of BC and model groups tended to differentiate. This suggested that the metabolites were shifted in the model group.

OPLS-DA showed that the BC and model groups could be distinguished clearly in both positive mode (Fig. A.4C) and negative mode (Fig. A.4E). The results of permutation tests suggested the OPLS-DA models were valid, as the blue regression line of the Q2-points was below zero. That is to say, the metabolites migrated significantly after modeling (Fig. A.4D and 4F). An S-plot (Fig. A.4G and 4H) was also constructed to visually reflect the contribution of each variable. Points farther from the original points contribute more to the difference. OPLS-DA models containing all samples were also established to observe the distance between groups. Points becoming closer suggested a more similar metabolic constitution. As shown in Fig. 4A and C, the five groups could be differentiated no matter whether in positive or negative mode, respectively. However, the three drug treatment groups all exhibited unsatisfactory regulation, as the points were farther from those of the BC group. In addition, a permutation plot of the model showed the same result (Fig. 4B and 4D).

A total of 17 significant metabolites were identified by histogram comparison (Fig. 5A and Table A4). As Fig. 5B and C shows, only six components (7a,12a-dihydroxy-3-oxo-4-cholenoic acid, 7-ketodeoxycholic acid, 3,4-methylenesebacic acid, 19,20-dihydroxydocosapentaenoic acid [19,20-DiHDPA], dihydrocortisol, and enterolactone) trended toward a return to the level of the BC group after AUMP treatment, whereas the other metabolites exhibited no significant change after AUMP treatment compared with the model group. This result suggests that these six metabolites play a critical role in treatment of HUA by AMUP.

In the feces metabolomics analysis, the content of the 3,4-methylenesebacic acid in rats with HUA decreased compared to the BC group. However, this trend was not observed in the other three drug treatment groups. 3,4-Methylenesebacic acid is a biomarker used to predict neutropenia (Deng et al. 2020). Neutrophils with a strong ability to kill pathogens are

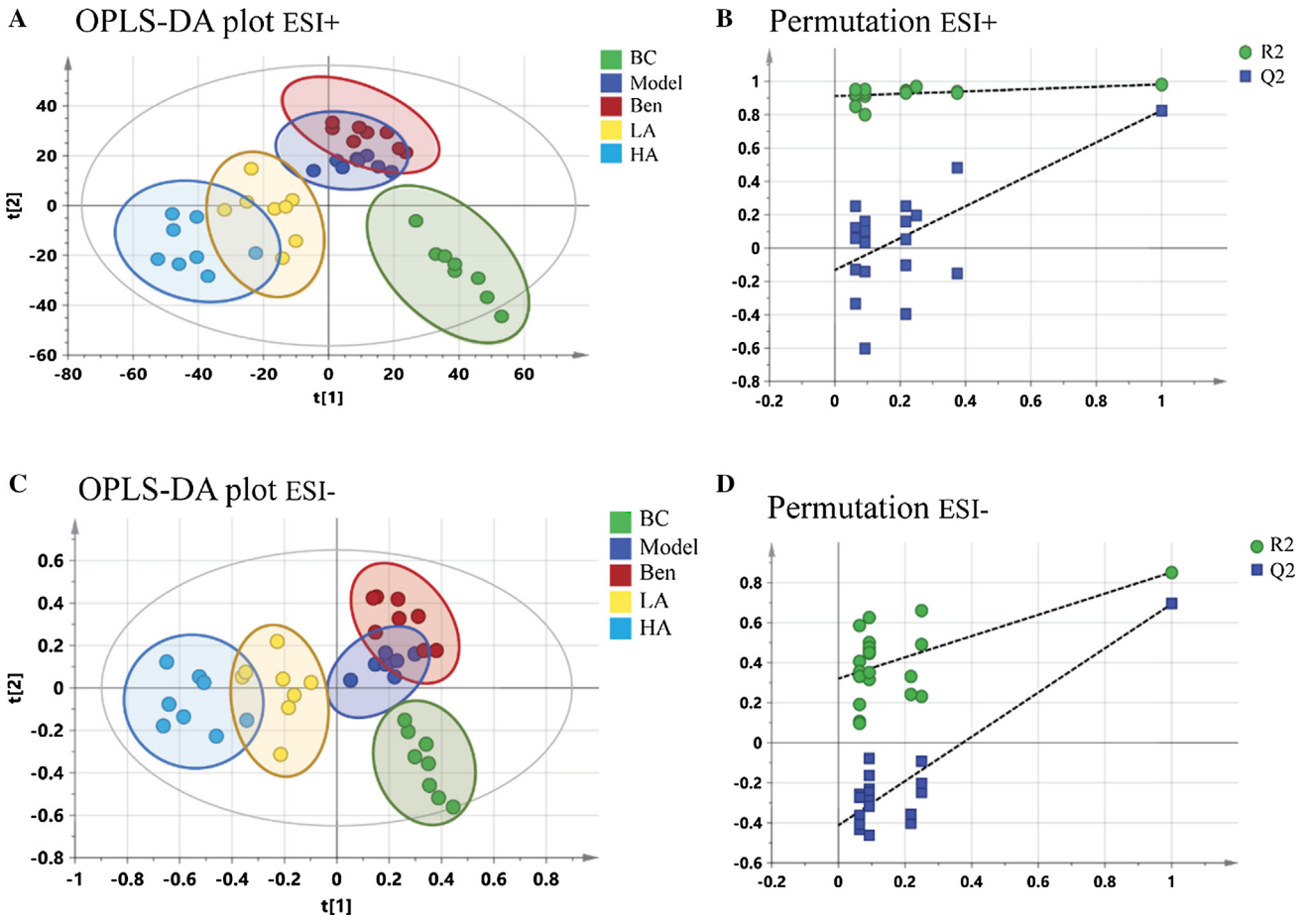


**Fig. 4** OPLS-DA plots and permutation tests for all samples. A-B, ESI + model. C-D, ESI-model.

the most abundant type of white blood cell in the peripheral blood. In addition, uric acid stimulates inflammation via the production of p38 mitogen–activated protein kinases, cyclooxygenase-2, and chemokine monocyte chemoattractant protein-1 (Darmawan et al. 2017). Therefore, fewer neutrophils in the intestine and high uric acid levels may increase the risk of intestinal inflammation in HUA patients. Further, after low-dose AMUP treatment, the level of 3,4-methylenesebacic acid returned to the same level as the control group, suggesting that AMUP treatment can increase the number of some immune cells in the rat intestine. Production of the n-3n-3 polyunsaturated fatty acid–derived diol metabolite 19,20-diHDPA is mediated by cytochrome P450. Increased 19,20-diHDPA levels are indicative of an anti-inflammatory profile (Heemskerk et al. 2014). However, in the intestine of rats with HUA, levels of 19,20-diHDPA were lower compared with the other three groups, which also suggests a higher risk of intestinal inflammation in HUA patients. Taken together, these data suggest that high uric acid levels reduce the number of various immune cells and anti-inflammatory factors in the intestine.

Uric acid amplifies the lipogenic effects of fructose by increasing ketohexokinase expression, which results in TG accumulation in hepatocytes (Lanaspa et al. 2012). Liver fat content accumulation increases the severity of non-alcoholic fatty liver disease (NAFLD) (Sirota et al. 2013), and NAFLD can increase the concentration of total bile acids and affect the metabolism of bile acids in the liver (Chavez-Talavera et al. 2017). Indeed, cholic acid was proposed as a potential mediator of liver injury (Smith et al. 2004), and its levels were higher in the rats of the model group than those of the control group. 7-Ketodeoxycholic acid and 7a,12a-dihydroxy-3-oxo-4-cholenoic acid are intermediates in the biotransformation of conjugates of cholic acid (3α,7α,12α-trihydroxy-5β-cholan-24-oic acid) and chenodeoxycholic acid (3α,7α-dihydroxy-5β-cho lan-24-oic acid) into the unconjugated secondary bile acids deoxycholic acid (3α,12α-dihydroxy-5β-cholan-24-oic acid) and lithocholic acid (3α-hydroxy-5β-cholan-24-oic acid) (Sutherland et al. 1984, Song et al. 2019, Quinn et al. 2020). As Fig. 5B shows, the level of both 7-ketodeoxycholic acid and 7a,12a-dihydroxy-3-oxo-4-cholenoic acid were significantly higher in the rats of the model group than the control group. In addition, pathway enrichment analysis showed that significant metabolites were enriched in the primary bile acid biosynthesis pathways, suggesting that HUA leads to hepatic injury and that AUMP treatment can alleviate such damage and reverse the dysregulation of bile acid biosynthesis pathways. HE staining consistently showed that liver tissue of the rats in the model group had pathological changes, and AUMP treatment reversed the liver damage caused by HUA.

Dihydrocortisol is a glucocorticoid secreted by the adrenal gland and plays a role in regulation of the hydro-salinity balance, glucose metabolism, and growth and development (Mikami et al. 1980, Kallubai et al. 2019). In addition, dihy-

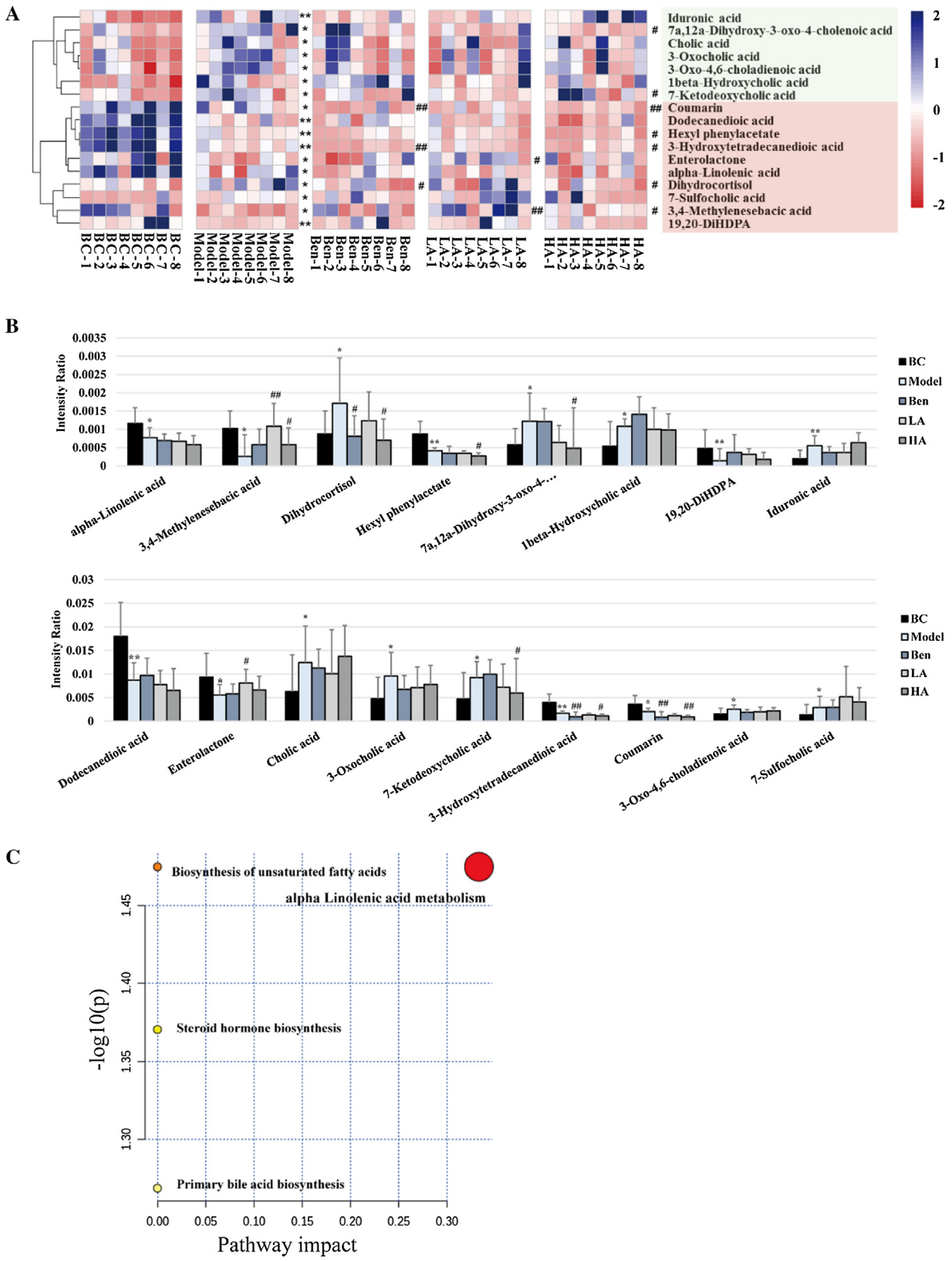


**Fig. 5** Metabolomic analysis of the effects of AMUP on HUA. A, Heatmap of differential metabolites that were altered in rats with HUA compared with normal rats. Deeper blue colored blocks represent higher content, whereas deeper red represents lower content. B, Intensity comparison of significant metabolites between the five groups. $*P < 0.05$ compared with BC group; $**P < 0.0$ L compared with BC group; $\#P < 0.05$ compared with model group; $\#\#P < 0.01$ compared with model group. C, Summary of pathway analysis. Pathway impact value calculated from pathway topology analysis; a small *P*-value and large pathway impact factor indicate the pathway was significantly affected.

drocortisol has anti-inflammatory effects and suppresses immune responses (Southren et al. 1985). Fecal metabolomics data indicated that in the intestine of model group rats, dihydrocortisol levels were higher than in the other three groups, suggesting that HUA damages the adrenal gland and causes adrenal cortical hyperplasia. Long-term dihydrocortisol excess leads to hypertension, abnormal glucose metabolism, centripetal obesity, and other symptoms, which may the reason why the weight of the rats in the model group with HUA was higher. We also found that the level of corticosterone in the serum of rats with HUA was significantly higher than that in the BC group. In addition, pathway analysis results indicated that steroid hormone biosynthesis may be affected by HUA (Fig. 5C), suggesting that hormone levels in patients with HUA are dysregulated.

As Fig. 5C indicates, the content of Enterolactone (EL) was reduced in the intestine of rats with HUA but returned to normal after drug treatment, especially treatment with low-dose AUMP. EL is a bioactive phenolic metabolite known as a mammalian lignan derived from dietary lignans. Different strains of microbes in the host gut are involved in the metabolic conversion of dietary lignans into EL (Halldin et al. 2019). Further studies have revealed that EL possesses potent protective properties against different cancers via mediation of different signaling pathways or immune factor release (Mali et al. 2019). In addition, EL affects the development of hepatocyte inflammation by modifying the fatty acid composition (Berk et al. 2019). Therefore, a high level of EL in the intestine may contribute to the remission of HUA.

## 4. Conclusions

HUA is a metabolic disease caused by excessive production of uric acid or excretion disorders of uric acid. Long-term high uric acid can lead to various syndromes, especially gout. In Western medicine, drugs are often used for the treatment of HUA. However, some reports show that chronic administration of Western drugs can have toxic side effects. *Astragalus membranaceus* is a medicinal herb commonly used in many herbal formulations in the practice of TCM to treat a wide variety of diseases and disorders (Auyeung et al. 2016). In this study, the potential use of AMUP and its chemical constituents in the treatment of HUA was investigated via 16S rRNA sequencing and metabolomics analyses.

We found that the effect of low-dose AMUP in alleviating HUA was better than that of the Western medicine benzbromarone and caused less damage to the kidney and liver. In addition, 16S rRNA sequencing of the intestinal microbiota indicated that low-dose AMUP can reverse the intestinal flora imbalance induced by HUA more effectively than benzbromarone or high-dose AMUP. Our results showed that low-dose AMUP has no toxic side effects and could therefore serve as a reference dose for the treatment of HUA. To explore which metabolic pathways or metabolites are affected by AMUP in alleviating HUA, we analyzed the fecal metabolome and found that the content of bile acid and its two downstream metabolites were significantly increased in the model group, perhaps because HUA can cause liver damage. However, low-dose AMUP reversed these increases. Moreover, the levels of some biomarkers related to immune cells and intestinal inflammatory responses in the model group were decreased, but these biomarkers returned to the level of the BC group after treatment with AMUP.

We also found that the secretion of some adrenal hormones important in the metabolism of basic substances (Byakodi et al. 2017, Gomes et al. 2020) was dysregulated in rats with HUA, suggesting that high uric acid levels may also lead to damage of the adrenal gland and affect the secretion of related hormones. Taking AMUP can help these hormones return to normal levels. Taken together, these data indicate that HUA holds great potential as a cure for HUA by reshaping the structure of the intestinal microbiota and stabilizing dysregulated metabolic pathways.

## Funding

This work was supported by National Natural Science Foundation of China (82174039); National Natural Science Foundation of Shandong Province (ZR2020MH371); Young and Creative Team for Talent Introduction of Shandong Province (10073004); Chinese herbal medicine and decoction piece standard research topic of Shandong Province (2020-201), Locality-University Cooperation Project of Yantai City (2019XDRHXMPT18).

## Authors' contributions

Jiayu Zhang and Wenwen Zhang designed the study. Wenwen Zhang, Zihan Liu and Yifang Cui performed the experiments, Wenwen Zhang and Jiayu Zhang drafted and revised the manuscript. Wenwen Zhang, Zihan Liu, Shaoping Wang, Ailin Yang and Yifang Cui analyzed and interpreted the data. All authors read and approved the final manuscript.

## Declaration of competing interest

None of the authors declare any conflicts of interest related this study.

## Acknowledgments

We would like to thank all the people who participated in this study.

## Appendix A. Supplementary material

Supplementary data to this article can be found online at https://doi.org/10.1016/j.arabjc.2022.103970.

## References

Alves-Bezerra, M., Cohen, D.E., 2017. Triglyceride Metabolism in the Liver. Compr. Physiol. 81, 1–8. https://doi.org/10.1002/cphy.c170012.

Auyeung, K.K., Han, Q.B., Ko, J.K., 2016. Astragalus membranaceus: A Review of its Protection Against Inflammation and Gastrointestinal Cancers. Am. J. Chin. Med. 441, 1–22. https://doi.org/10.1142/S0192415X16500014.

Baker, S., The, H.C., 2018. Recent insights into Shigella. Curr. Opin. Infect. Dis. 315, 449–454. https://doi.org/10.1097/QCO.0000000000000475.

Berk, K., Drygalski, K., Harasim-Symbor, E., Charytoniuk, T., Ilowska, N., Lukaszuk, B., Chabowski, A., Konstantynowicz-Nowicka, K., 2019. The effect of enterolactone on liver lipid precursors of inflammation. Life Sci. 221, 341–347. https://doi.org/10.1016/j.lfs.2019.02.044.

Byakodi, S., Gurjar, V., Soni, S., 2017. Glucose Levels and Hemodynamic Changes in Patients submitted to Routine Dental Extraction under Local Anesthesia with and without Adrenaline. J. Contemp. Dent. Pract. 181, 57–59. https://doi.org/10.5005/jp-journals-10024-1989.

Chavez-Talavera, O., Tailleux, A., Lefebvre, P., Staels, B., 2017. Bile Acid Control of Metabolism and Inflammation in Obesity, Type 2 Diabetes, Dyslipidemia, and Nonalcoholic Fatty Liver Disease. Gastroenterology 1527, (1679–1694). https://doi.org/10.1053/j.gastro.2017.01.055 e1673.

Chen, L., Wilson, J.E., Koenigsknecht, M.J., Chou, W.C., Montgomery, S.A., Truax, A.D., Brickey, W.J., Packey, C.D., Maharshak, N., Matsushima, G.K., Plevy, S.E., Young, V.B., Sartor, R. B., Ting, J.P., 2017. NLRP12 attenuates colon inflammation by maintaining colonic microbial diversity and promoting protective commensal bacterial growth. Nat. Immunol. 185, 541–551. https://doi.org/10.1038/ni.3690.

Chen, R., Wang, J., Zhan, R., Zhang, L., Wang, X., 2019. Fecal metabonomics combined with 16S rRNA gene sequencing to analyze the changes of gut microbiota in rats with kidney-yang deficiency syndrome and the intervention effect of You-gui pill. J. Ethnopharmacol. 244,. https://doi.org/10.1016/j.jep.2019.112139 112139.

Cote, J.M., Berube, A.A., Bollee, G., 2020. Association of Hyperuricemia With Acute Kidney Injury: Case Series Report Among Patients Hospitalized With General Tonic-Clonic Seizures. Can. J. Kidney Health Dis. 7. https://doi.org/10.1177/2054358120977386. 2054358120977386.

Darmawan, G., Hamijoyo, L., Hasan, I., 2017. Association between Serum Uric Acid and Non-Alcoholic Fatty Liver Disease: A Meta-Analysis. Acta Med. Indones. 492, 136–147.

Deng, Y., Yao, H., Chen, W., Wei, H., Li, X., Zhang, F., Gao, S., Man, H., Chen, J., Tao, X., Li, M., Chen, W., 2020. Profiling of polar urine metabolite extracts from Chinese colorectal cancer patients to screen for potential diagnostic and adverse-effect biomarkers. J. Cancer 1123, 6925–6938. https://doi.org/10.7150/jca.47631.

Fischer, A.H., Jacobson, K.A., Rose, J., Zeller, R., 2008. Hematoxylin and eosin staining of tissue and cell sections. CSH Protoc 2008, pdb prot4986. https://doi.org/10.1101/pdb.prot4986.

Fu, J., Wang, Z., Huang, L., Zheng, S., Wang, D., Chen, S., Zhang, H., Yang, S., 2014. Review of the botanical characteristics, phytochemistry, and pharmacology of Astragalus membranaceus (Huangqi). Phytother. Res. 289, 1275–1283. https://doi.org/10.1002/ptr.5188.

Gomes, A., Soares, R., Costa, R., Marino, F., Cosentino, M., Malagon, M.M., Ribeiro, L., 2020. High-fat diet promotes adrenaline production by visceral adipocytes. Eur. J. Nutr. 593, 1105–1114. https://doi.org/10.1007/s00394-019-01971-0.

Halldin, E., Eriksen, A.K., Brunius, C., da Silva, A.B., Bronze, M., Hanhineva, K., Aura, A.M., Landberg, R., 2019. Factors Explaining Interpersonal Variation in Plasma Enterolactone Concentrations in Humans. Mol. Nutr. Food Res. 6316,. https://doi.org/10.1002/mnfr.201801159 e1801159.

Heemskerk, M.M., Dharuri, H.K., van den Berg, S.A., Jonasdottir, H. S., Kloos, D.P., Giera, M., van Dijk, K.W., van Harmelen, V., 2014. Prolonged niacin treatment leads to increased adipose tissue PUFA synthesis and anti-inflammatory lipid and oxylipin plasma profile. J. Lipid Res. 5512, 2532–2540. https://doi.org/10.1194/jlr.M051938.

Hong, G.U., Lee, J.Y., Kang, H., Kim, T.Y., Park, J.Y., Hong, E.Y., Shin, Y.H., Jung, S.H., Chang, H.B., Kim, Y.H., Kwon, Y.I., Ro, J.Y., 2018. Inhibition of Osteoarthritis-Related Molecules by Isomucronulatol 7-O-beta-d-glucoside and Ecliptasaponin A in IL-1beta-Stimulated Chondrosarcoma Cell Model. Molecules 2311. https://doi.org/10.3390/molecules23112807.

Hosseini, E., Grootaert, C., Verstraete, W., Van de Wiele, T., 2011. Propionate as a health-promoting microbial metabolite in the human gut. Nutr. Rev. 695, 245–258. https://doi.org/10.1111/j.1753-4887.2011.00388.x.

Hu, C., Wu, X., 2019. Treatment of asymptomatic hyperuricemia complicated by renal damage: a controversial issue. Int. Urol. Nephrol. 5112, 2227–2233. https://doi.org/10.1007/s11255-019-02256-5.

Johnson, J.S., Spakowicz, D.J., Hong, B.Y., Petersen, L.M., Demkowicz, P., Chen, L., Leopold, S.R., Hanson, B.M., Agresta, H.O., Gerstein, M., Sodergren, E., Weinstock, G.M., 2019. Evaluation of 16S rRNA gene sequencing for species and strain-level microbiome analysis. Nat. Commun. 101, 5029. https://doi.org/10.1038/s41467-019-13036-1.

Kallubai, M., Reddy, S.P., Dubey, S., Ramachary, D.B., Subramanyam, R., 2019. Spectroscopic evaluation of synthesized 5beta-dihydrocortisol and 5beta-dihydrocortisol acetate binding mechanism with human serum albumin and their role in anticancer activity. J. Biomol. Struct. Dyn. 373, 623–640. https://doi.org/10.1080/07391102.2018.1433554.

Kim, D.H., 2018. Gut microbiota-mediated pharmacokinetics of ginseng saponins. J. Ginseng Res. 423, 255–263. https://doi.org/10.1016/j.jgr.2017.04.011.

Kong, C., Gao, R., Yan, X., Huang, L., Qin, H., 2019. Probiotics improve gut microbiota dysbiosis in obese mice fed a high-fat or high-sucrose diet. Nutrition 60, 175–184. https://doi.org/10.1016/j.nut.2018.10.002.

Kwo, P.Y., Cohen, S.M., Lim, J.K., 2017. ACG Clinical Guideline: Evaluation of Abnormal Liver Chemistries. Am. J. Gastroenterol. 1121, 18–35. https://doi.org/10.1038/ajg.2016.517.

Lains, I., Gantner, M., Murinello, S., Lasky-Su, J.A., Miller, J.W., Friedlander, M., Husain, D., 2019. Metabolomics in the study of retinal health and disease. Prog. Retin. Eye Res. 69, 57–79. https://doi.org/10.1016/j.preteyeres.2018.11.002.

Lanaspa, M.A., Sanchez-Lozada, L.G., Cicerchi, C., Li, N., Roncal-Jimenez, C.A., Ishimoto, T., Le, M., Garcia, G.E., Thomas, J.B., Rivard, C.J., Andres-Hernando, A., Hunter, B., Schreiner, G., Rodriguez-Iturbe, B., Sautin, Y.Y., Johnson, R.J., 2012. Uric acid stimulates fructokinase and accelerates fructose metabolism in the development of fatty liver. PLoS ONE 710,. https://doi.org/10.1371/journal.pone.0047948 e47948.

Le Gall, G., Noor, S.O., Ridgway, K., Scovell, L., Jamieson, C., Johnson, I.T., Colquhoun, I.J., Kemsley, E.K., Narbad, A., 2011. Metabolomics of fecal extracts detects altered metabolic activity of gut microbiota in ulcerative colitis and irritable bowel syndrome. J. Proteome Res. 109, 4208–4218. https://doi.org/10.1021/pr2003598.

Li, C., Li, Z., Liu, S., Wang, C., Han, L., Cui, L., Zhou, J., Zou, H., Liu, Z., Chen, J., Cheng, X., Zhou, Z., Ding, C., Wang, M., Chen, T., Cui, Y., He, H., Zhang, K., Yin, C., Wang, Y., Xing, S., Li, B., Ji, J., Jia, Z., Ma, L., Niu, J., Xin, Y., Liu, T., Chu, N., Yu, Q., Ren, W., Wang, X., Zhang, A., Sun, Y., Wang, H., Lu, J., Li, Y., Qing, Y., Chen, G., Wang, Y., Zhou, L., Niu, H., Liang, J., Dong, Q., Li, X., Mi, Q.S., Shi, Y., 2015. Genome-wide association analysis identifies three new risk loci for gout arthritis in Han Chinese. Nat. Commun. 6, 7041. https://doi.org/10.1038/ncomms8041.

Li, M., Wang, W., Xue, J., Gu, Y., Lin, S., 2011. Meta-analysis of the clinical value of Astragalus membranaceus in diabetic nephropathy. J. Ethnopharmacol. 1332, 412–419. https://doi.org/10.1016/j.jep.2010.10.012.

Li, X., Yan, Z., Tian, J., Zhang, X., Han, H., Ye, F., 2019. Urate Transporter URAT1 in Hyperuricemia: New Insights from Hyperuricemic Models. Ann. Clin. Lab. Sci. 496, 756–762.

Lin, Y., Vonk, R.J., Slooff, M.J., Kuipers, F., Smit, M.J., 1995. Differences in propionate-induced inhibition of cholesterol and

triacylglycerol synthesis between human and rat hepatocytes in primary culture. Br. J. Nutr. 742, 197–207. https://doi.org/10.1079/bjn19950123.

Liu, B., Zhao, L., Yang, Q., Zha, D., Si, X., 2021. Hyperuricemia and hypertriglyceridemia indicate tubular atrophy/interstitial fibrosis in patients with IgA nephropathy and membranous nephropathy. Int. Urol. Nephrol. https://doi.org/10.1007/s11255-021-02844-4.

Liu, G., Pilla, G., Tang, C.M., 2019. Shigella host: Pathogen interactions: Keeping bacteria in the loop. Cell. Microbiol. 2111,. https://doi.org/10.1111/cmi.13062 e13062.

Liu, P., Zhao, H., Luo, Y., 2017. Anti-Aging Implications of Astragalus Membranaceus (Huangqi): A Well-Known Chinese Tonic. Aging Dis. 86, 868–886. https://doi.org/10.14336/AD.2017.0816.

Liu, X., Lv, Q., Ren, H., Gao, L., Zhao, P., Yang, X., Yang, G., Xu, D., Wang, G., Yang, W., Wang, P., Wang, Z., Xing, S., 2020. The altered gut microbiota of high-purine-induced hyperuricemia rats and its correlation with hyperuricemia. PeerJ 8,. https://doi.org/10.7717/peerj.8664 e8664.

Lu, H., 2007. Stereoselectivity in drug metabolism. Expert Opin. Drug Metab. Toxicol. 32, 149–158. https://doi.org/10.1517/17425255.3.2.149.

Lyu, M., Wang, Y.F., Fan, G.W., Wang, X.Y., Xu, S.Y., Zhu, Y., 2017. Balancing Herbal Medicine and Functional Food for Prevention and Treatment of Cardiometabolic Diseases through Modulating Gut Microbiota. Front. Microbiol. 8, 2146. https://doi.org/10.3389/fmicb.2017.02146.

Mali, A.V., Padhye, S.B., Anant, S., Hegde, M.V., Kadam, S.S., 2019. Anticancer and antimetastatic potential of enterolactone: Clinical, preclinical and mechanistic perspectives. Eur. J. Pharmacol. 852, 107–124. https://doi.org/10.1016/j.ejphar.2019.02.022.

Meehan, C.J., Beiko, R.G., 2014. A phylogenomic view of ecological specialization in the Lachnospiraceae, a family of digestive tract-associated bacteria. Genome Biol. Evol. 63, 703–713. https://doi.org/10.1093/gbe/evu050.

Mikami, H., Nugent, C.A., Ogihara, T., Naka, T., Iwanaga, K., Kumahara, Y., 1980. The effect of 5 alpha-dihydrocortisol on the blood pressure of rats treated with deoxycorticosterone acetate and salt. Endocrinol. Jpn. 276, 769–773. https://doi.org/10.1507/endocrj1954.27.769.

Milovic, V., Teller, I.C., Turchanowa, L., Caspary, W.F., Stein, J., 2000. Effect of structural analogues of propionate and butyrate on colon cancer cell growth. Int. J. Colorectal Dis. 155–6, 264–270. https://doi.org/10.1007/s003840000257.

Minton, N.P., 2003. Clostridia in cancer therapy. Nat. Rev. Microbiol. 13, 237–242. https://doi.org/10.1038/nrmicro777.

Murea, M., 2012. Advanced kidney failure and hyperuricemia. Adv. Chronic Kidney Dis. 196, 419–424. https://doi.org/10.1053/j.ackd.2012.07.008.

Nishina, P.M., Freedland, R.A., 1990. Effects of propionate on lipid biosynthesis in isolated rat hepatocytes. J. Nutr. 1207, 668–673. https://doi.org/10.1093/jn/120.7.668.

Pedersen, H.K., Gudmundsdottir, V., Nielsen, H.B., Hyotylainen, T., Nielsen, T., Jensen, B.A., Forslund, K., Hildebrand, F., Prifti, E., Falony, G., Le Chatelier, E., Levenez, F., Dore, J., Mattila, I., Plichta, D.R., Poho, P., Hellgren, L.I., Arumugam, M., Sunagawa, S., Vieira-Silva, S., Jorgensen, T., Holm, J.B., Trost, K., Meta, H.I. T.C., Kristiansen, K., Brix, S., Raes, J., Wang, J., Hansen, T., Bork, P., Brunak, S., Oresic, M., Ehrlich, S.D., Pedersen, O., 2016. Human gut microbes impact host serum metabolome and insulin sensitivity. Nature 5357612, 376–381. https://doi.org/10.1038/nature18646.

Qi, X., Tester, R.F., 2019. Fructose, galactose and glucose - In health and disease. Clin. Nutr. ESPEN 33, 18–28. https://doi.org/10.1016/j.clnesp.2019.07.004.

Qin, J., Li, Y., Cai, Z., Li, S., Zhu, J., Zhang, F., Liang, S., Zhang, W., Guan, Y., Shen, D., Peng, Y., Zhang, D., Jie, Z., Wu, W., Qin, Y., Xue, W., Li, J., Han, L., Lu, D., Wu, P., Dai, Y., Sun, X., Li, Z., Tang, A., Zhong, S., Li, X., Chen, W., Xu, R., Wang, M., Feng, Q., Gong, M., Yu, J., Zhang, Y., Zhang, M., Hansen, T., Sanchez, G., Raes, J., Falony, G., Okuda, S., Almeida, M., LeChatelier, E., Renault, P., Pons, N., Batto, J.M., Zhang, Z., Chen, H., Yang, R., Zheng, W., Li, S., Yang, H., Wang, J., Ehrlich, S.D., Nielsen, R., Pedersen, O., Kristiansen, K., Wang, J., 2012. A metagenome-wide association study of gut microbiota in type 2 diabetes. Nature 4907418, 55–60. https://doi.org/10.1038/nature11450.

Quinn, R.A., Melnik, A.V., Vrbanac, A., Fu, T., Patras, K.A., Christy, M.P., Bodai, Z., Belda-Ferre, P., Tripathi, A., Chung, L.K., Downes, M., Welch, R.D., Quinn, M., Humphrey, G., Panitchpakdi, M., Weldon, K.C., Aksenov, A., da Silva, R., Avila-Pacheco, J., Clish, C., Bae, S., Mallick, H., Franzosa, E.A., Lloyd-Price, J., Bussell, R., Thron, T., Nelson, A.T., Wang, M., Leszczynski, E., Vargas, F., Gauglitz, J.M., Meehan, M.J., Gentry, E., Arthur, T.D., Komor, A.C., Poulsen, O., Boland, B.S., Chang, J.T., Sandborn, W.J., Lim, M., Garg, N., Lumeng, J.C., Xavier, R. J., Kazmierczak, B.I., Jain, R., Egan, M., Rhee, K.E., Ferguson, D., Raffatellu, M., Vlamakis, H., Haddad, G.G., Siegel, D., Huttenhower, C., Mazmanian, S.K., Evans, R.M., Nizet, V., Knight, R., Dorrestein, P.C., 2020. Global chemical effects of the microbiome include new bile-acid conjugations. Nature 5797797, 123–129. https://doi.org/10.1038/s41586-020-2047-9.

Sanchez, B., Delgado, S., Blanco-Miguez, A., Lourenco, A., Gueimonde, M., Margolles, A., 2017. Probiotics, gut microbiota, and their influence on host health and disease. Mol. Nutr. Food Res. 611. https://doi.org/10.1002/mnfr.201600240.

Shu, S.A., Yuen, A.W.T., Woo, E., Chu, K.H., Kwan, H.S., Yang, G. X., Yang, Y., Leung, P.S.C., 2019. Microbiota and Food Allergy. Clin. Rev. Allergy Immunol. 571, 83–97. https://doi.org/10.1007/s12016-018-8723-y.

Sibai, M., Altuntas, E., Yildirim, B., Ozturk, G., Yildirim, S., Demircan, T., 2020. Microbiome and Longevity: High Abundance of Longevity-Linked Muribaculaceae in the Gut of the Long-Living Rodent Spalax leucodon. OMICS 2410, 592–601. https://doi.org/10.1089/omi.2020.0116.

Sinclair, S., 1998. Chinese herbs: a clinical review of Astragalus, Ligusticum, and Schizandrae. Altern. Med. Rev. 35, 338–344.

Sirota, J.C., McFann, K., Targher, G., Johnson, R.J., Chonchol, M., Jalal, D.I., 2013. Elevated serum uric acid levels are associated with non-alcoholic fatty liver disease independently of metabolic syndrome features in the United States: Liver ultrasound data from the National Health and Nutrition Examination Survey. Metabolism 623, 392–399. https://doi.org/10.1016/j.metabol.2012.08.013.

Smith, B.J., Miller, R.A., Ericsson, A.C., Harrison, D.C., Strong, R., Schmidt, T.M., 2019. Changes in the gut microbiome and fermentation products concurrent with enhanced longevity in acarbose-treated mice. BMC Microbiol. 191, 130. https://doi.org/10.1186/s12866-019-1494-7.

Smith, J.L., Lewindon, P.J., Hoskins, A.C., Pereira, T.N., Setchell, K. D., O'Connell, N.C., Shepherd, R.W., Ramm, G.A., 2004. Endogenous ursodeoxycholic acid and cholic acid in liver disease due to cystic fibrosis. Hepatology 396, 1673–1682. https://doi.org/10.1002/hep.20238.

Song, Y., Shan, B., Li, H., Feng, B., Peng, H., Jin, C., Xu, P., Zeng, Q., Liao, Z., Mu, P., Su, D., 2019. Safety investigation of Pulsatilla chinensis saponins from chronic metabonomic study of serum biomedical changes in oral treated rat. J. Ethnopharmacol. 235, 435–445. https://doi.org/10.1016/j.jep.2019.01.035.

Southren, A.L., Gordon, G.G., l'Hommedieu, D., Ravikumar, S., Dunn, M.W., Weinstein, B.I., 1985. 5 beta-Dihydrocortisol: possible mediator of the ocular hypertension in glaucoma. Invest. Ophthalmol. Vis. Sci. 263, 393–395.

Sutherland, J.D., Holdeman, L.V., Williams, C.N., Macdonald, I.A., 1984. Formation of urso- and ursodeoxy-cholic acids from primary bile acids by a Clostridium limosum soil isolate. J. Lipid Res. 2510, 1084–1089.

Tang, W.H., Kitai, T., Hazen, S.L., 2017. Gut Microbiota in Cardiovascular Health and Disease. Circ. Res. 1207, 1183–1196. https://doi.org/10.1161/CIRCRESAHA.117.309715.

Teixeira, L.D., Kling, D.N., Lorca, G.L., Gonzalez, C.F., 2018. Lactobacillus johnsonii N6.2 diminishes caspase-1 maturation in the gastrointestinal system of diabetes prone rats. Benef. Microbes 93, 527–539. https://doi.org/10.3920/BM2017.0120.

Ussar, S., Griffin, N.W., Bezy, O., Fujisaka, S., Vienberg, S., Softic, S., Deng, L., Bry, L., Gordon, J.I., Kahn, C.R., 2015. Interactions between Gut Microbiota, Host Genetics and Diet Modulate the Predisposition to Obesity and Metabolic Syndrome. Cell Metab. 223, 516–530. https://doi.org/10.1016/j.cmet.2015.07.007.

Ussher, J.R., Elmariah, S., Gerszten, R.E., Dyck, J.R., 2016. The Emerging Role of Metabolomics in the Diagnosis and Prognosis of Cardiovascular Disease. J. Am. Coll. Cardiol. 6825, 2850–2870. https://doi.org/10.1016/j.jacc.2016.09.972.

Wallace, J.G., Bellissimo, C.J., Yeo, E., Fei Xia, Y., Petrik, J.J., Surette, M.G., Bowdish, D.M.E., Sloboda, D.M., 2019. Obesity during pregnancy results in maternal intestinal inflammation, placental hypoxia, and alters fetal glucose metabolism at mid-gestation. Sci. Rep. 91, 17621. https://doi.org/10.1038/s41598-019-54098-x.

Wang, Z., Zhao, Y., 2018. Gut microbiota derived metabolites in cardiovascular health and disease. Protein Cell 95, 416–431. https://doi.org/10.1007/s13238-018-0549-0.

Wikoff, W.R., Anfora, A.T., Liu, J., Schultz, P.G., Lesley, S.A., Peters, E.C., Siuzdak, G., 2009. Metabolomics analysis reveals large effects of gut microflora on mammalian blood metabolites. Proc. Natl. Acad. Sci. U. S. A. 10610, 3698–3703. https://doi.org/10.1073/pnas.0812874106.

Xu, G.H., Yuan, L., Li, Y., Xie, P., Zhao, J.Y., Chen, Y.H., 2008. Clinical observation of Astragalus Injection in treatment of renal injury in patients with primary hypertension. Zhong Xi Yi Jie He Xue Bao 65, 530–532. https://doi.org/10.3736/jcim20080519.

Xu, Y., Wang, N., Tan, H.Y., Li, S., Zhang, C., Zhang, Z., Feng, Y., 2020. Panax notoginseng saponins modulate the gut microbiota to promote thermogenesis and beige adipocyte reconstruction via leptin-mediated AMPKalpha/STAT3 signaling in diet-induced obesity. Theranostics 1024, 11302–11323. https://doi.org/10.7150/thno.47746.

Yang, F., Qu, Q., Zhao, C., Liu, X., Yang, P., Li, Z., Han, L., Shi, X., 2020. Paecilomyces cicadae-fermented Radix astragali activates podocyte autophagy by attenuating PI3K/AKT/mTOR pathways to protect against diabetic nephropathy in mice. Biomed. Pharmacother. 129,. https://doi.org/10.1016/j.biopha.2020.110479 110479.

Ye, X., Wu, J., Tang, K., Li, W., Xiong, C., Zhuo, L., 2019. Benzbromarone as a possible cause of acute kidney injury in patients with urolithiasis: Two case reports. Medicine (Baltimore) 9815,. https://doi.org/10.1097/MD.0000000000015214 e15214.

Yokota, A., Fukiya, S., Islam, K.B., Ooka, T., Ogura, Y., Hayashi, T., Hagio, M., Ishizuka, S., 2012. Is bile acid a determinant of the gut microbiota on a high-fat diet? Gut Microbes 35, 455–459. https://doi.org/10.4161/gmic.21216.

Zhang, M.Y., Niu, J.Q., Wen, X.Y., Jin, Q.L., 2019. Liver failure associated with benzbromarone: A case report and review of the literature. World J. Clin. Cases 713, 1717–1725. https://doi.org/10.12998/wjcc.v7.i13.1717.

Zhao, M., Tao, J., Du, L., Jiang, S., Qian, D., Duan, J., 2017. UPLC-Q-TOF/MS-Based Metabolic Profiling Comparison of Two Major Bioactive Components and Their Metabolites in Normal and CKD Rat Plasma, Urine and Feces Following Oral Administration of Fructus Corni Extract. J. Chromatogr. Sci. 558, 857–865. https://doi.org/10.1093/chromsci/bmx046.

Zhao, Q., Yang, W.R., Wang, X.H., Li, G.Q., Xu, L.Q., Cui, X., Liu, Y., Zuo, X.L., 2019. Clostridium butyricum alleviates intestinal low-grade inflammation in TNBS-induced irritable bowel syndrome in mice by regulating functional status of lamina propria dendritic cells. World J. Gastroenterol. 2536, 5469–5482. https://doi.org/10.3748/wjg.v25.i36.5469.